NJC

PAPER

View Article Online
View Journal | View Issue

Cite this: *New J. Chem.*, 2017, **41**, 6232

A new rod-shaped BODIPY-acetylene molecule for solution-processed semiconducting microribbons in n-channel organic field-effect transistors†

Mehmet Ozdemir,[a] Donghee Choi,[b] Yunus Zorlu,[c] Bunyemin Cosut,[c] Hyungsug Kim,[b] Choongik Kim*[b] and Hakan Usta*[a]

BODIPY-based π-conjugated small molecules have been extensively studied in various fields of sensing and biochemical labelling; however, their use in organic optoelectronic applications is very limited. A new solution-processable acceptor–donor–acceptor (A–D–A) type small molecule, **BDY-PhAc-BDY**, consisting of BODIPY π-acceptors and a rod-shaped 1,4-bis-(thienylethynyl)2,5-dialkoxybenzene π-donor, has been synthesized and fully characterized as a novel n-channel semiconductor in bottom-gate/top-contact organic field-effect transistors (OFETs). The new semiconductor exhibits an electrochemical band gap of 2.12 eV with highly stabilized HOMO/LUMO energy levels of −5.68 eV/−3.56 eV. Single-crystal X-ray diffraction (XRD) analysis of **BDY-PhAc-BDY** reveals a relatively low "BODIPY-*meso*-thiophene" dihedral angle (θ = 44.94°), antiparallel π-stacked BODIPY dimers with an interplanar distance of 3.93 Å, and strong "C–H···π (2.85 Å)" interactions. The OFET devices fabricated by solution processing show the formation of highly-crystalline, one-dimensional (1-D) microribbons, which results in clear n-channel semiconductivity with an electron mobility of 0.004 $cm^2 V^{-1} s^{-1}$ and an on/off current ratio of 10^5–10^6. To date, this is the highest reported for BODIPY-based small molecular semiconductors with alkyne linkages. Our results clearly demonstrate that BODIPY is an effective π-acceptor unit for the design of solution-processable, electron-transporting organic semiconductors and easily fabricable 1-D semiconductor micro-/nano-structures for fundamental/applied research in organic optoelectronics.

Received 21st January 2017,
Accepted 27th May 2017

DOI: 10.1039/c7nj00266a

rsc.li/njc

Introduction

Solution-processable π-conjugated small molecules allow for the fabrication of thin, low-weight, and flexible organic optoelectronic devices such as field-effect transistors (OFETs),[1] light-emitting transistors (OLETs),[2] and photovoltaics (OPVs).[3] They offer significant physical/chemical advantages over their inorganic counterparts, including low cost, compatibility with flexible substrates and the roll-to-roll printing process, and structural versatility.[4–7] In the past several decades, the major advances in the performances of organic optoelectronic devices have been mainly due to the development of novel semiconducting structures employing properly designed π-architectures and the detailed understanding of their optoelectronic properties.[8–14] Therefore, continued research efforts in the search for new semiconductor π-structures and elucidation of the structure–property–device performance relationships are critical to developing novel optoelectronic platforms with varied functionalities. To this end, 4,4-difluoro-4-bora-3*a*,4*a*-diaza-*s*-indacene (BODIPY) remains a relatively unexplored π-core for use in semiconductor structures, despite the fact that it has been extensively studied in the past decades as a highly fluorescent functional dye for chemosensors, fluorescent switches and biochemical labels.[15] BODIPY is a coplanar and highly electron-deficient π-core with a high dipole moment (μ = 3.4–4.2 D), which makes it an ideal π-acceptor unit for the construction of donor–acceptor type semiconductor architectures.[16,17] Furthermore, considering its excellent photophysical and photochemical properties, BODIPY-based semiconductors would be ideal functional materials for light-based optoelectronic applications such as OLETs and OPVs.[18] However, to date there have been very few reports on BODIPY-based

[a] *Department of Materials Science and Nanotechnology Engineering, Abdullah Gül University, Kayseri, Turkey. E-mail: hakan.usta@agu.edu.tr*
[b] *Department of Chemical and Biomolecular Engineering, Sogang University, Mapo-gu, Seoul, Korea. E-mail: choongik@sogang.ac.kr*
[c] *Department of Chemistry, Gebze Technical University, Gebze, Kocaeli, Turkey*

† Electronic supplementary information (ESI) available: The ESI includes Fig. S1–S7 ($^1H/^{13}C$ NMR spectra and MALDI-TOF spectra for the intermediate compounds and the final small molecule), Fig. S8 (PL spectra of **BDY-PhAc-BDY**), Fig. S9 (simulated XRD powder pattern of **BDY-PhAc-BDY**), Fig. S10 (output plot for the OFET devices) and Table S1. CCDC 1482958 (for **BDY-PhAc-BDY**). For ESI and crystallographic data in CIF or other electronic format see DOI: 10.1039/c7nj00266a

semiconductor small molecules for optoelectronics with typical charge carrier mobilities of 10^{-5}–10^{-3} cm^2 V^{-1} s^{-1}.[19] To this end, our recent study revealed that properly designed A–D–A (acceptor–donor–acceptor) molecular π-architectures employing a BODIPY acceptor unit can induce n-channel semiconductivity with electron mobilities of up to ~0.01 cm^2 V^{-1} s^{-1} and I_{on}/I_{off} ratios of 10^7–10^8, which is the highest performance reported to date for a BODIPY-based semiconductor molecule.[20] Motivated by our initial promising findings, and to elucidate the full potential of the BODIPY π-core in electron-transporting molecules, we are interested in pursuing new BODIPY-based A–D–A π-architectures and exploring their semiconducting characteristics in n-channel OFETs.

In this paper, we report the synthesis, characterization, and field-effect response of a novel n-channel semiconductor molecule, **BDY-PhAc-BDY** (Fig. 1). In this structure, a rod-shaped 1,4-bis-(thienylethynyl)2,5-dialkoxybenzene π-architecture employs 2-ethylhexyloxy electron-donating groups on the central phenyl ring and terminal highly electron-deficient BODIPY π-units. Alkyne linkages are employed between the sterically-bulky central phenyl core and the thienyl units as a spacer to result in a shape-persistent rod-like structure with a further extended effective π-conjugation length.[21] Note that due to its quasi-cylindrical electronic symmetry, alkyne linkages are advantageous to accommodate steric and conformational constraints.[22] The rationale of having BODIPYs linked to five-membered thiophene units from their meso positions is to minimize inter-ring torsions between the donor and acceptor units, and to extend π-conjugation along the molecular backbone. Furthermore, 2-ethylhexyloxy lipophilic substituents provide the required solubility in common organic solvents for convenient purification and thin-film fabrication. A donor–acceptor backbone provides a low optical band gap of 2.2 eV with a relatively stabilized LUMO/HOMO energy level of −3.56/−5.68 eV for unipolar n-channel semiconductivity. Single-crystal X-ray diffraction (XRD) analysis shows important structural features of the new semiconductor. The solution-processed **BDY-PhAc-BDY**-based devices exhibit μ_e = 0.004 cm^2 V^{-1} s^{-1} with I_{on}/I_{off} ratios of 10^5–10^6, which is the highest OFET performance reported so far for BODIPY-based small molecules with alkyne linkages. Detailed morphological and microstructural thin-film analysis reveals the formation of highly crystalline one-dimensional (1-D) microribbons ([010] in the out-of-plane direction) as a result of favorable "–CH···π" and "π···π" intermolecular interactions. Our results clearly offer crucial guidance for the molecular design of BODIPY-based semiconductor molecules and easily fabricable microribbon-based thin-films for n-channel OFETs.

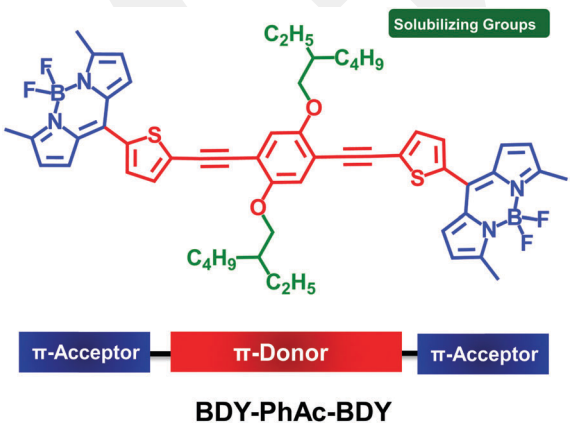

Fig. 1 Chemical structure of **BDY-PhAc-BDY**, as developed in this study, indicating the donor, acceptor, and solubilizing parts.

Experimental

Materials and methods

Schlenk techniques were used in the reactions, and the reactions were carried out under N_2 unless otherwise noted. All reagents were obtained from commercial sources and used without any purification unless otherwise noted. $^1H/^{13}C$ NMR characterizations were performed using a Bruker 400 spectrometer (^1H, 400 MHz; ^{13}C, 100 MHz). Elemental analyses were performed using a LecoTruspec Micro model instrument. MALDI-TOF was performed using a Bruker Microflex LT MALDI-TOF-MS Instrument. Thermogravimetric analysis (TGA) and differential scanning calorimetry (DSC) measurements were performed using Perkin Elmer Diamond model instruments at a heating rate of 10 °C min^{-1} under nitrogen. UV-Vis absorption and fluorescence emission measurements were performed using a Shimadzu, UV-1800 UV-Vis spectrophotometer and a varian eclipse spectrofluorometer, respectively. The fluorescence quantum yield was determined in dichloromethane as compared to the fluorescence of rhodamine 6G standart (Φ_F = 0.76 in water). Electrochemistry was performed on a C3 cell stand electrochemical station equipped with BAS-Epsilon software (Bioanalytical Systems, Inc. Lafayette, IN). The molecular geometry optimizations and total energy calculations were carried out using density functional theory (DFT) at the B3LYP/6-31G** level using Gaussian 09.[23]

Synthesis and characterization

Synthesis of the 5-bromo-2-thiophenecarbaldehyde and 2-methylpyrrole reagents was performed in accordance with our previously reported procedures.[20]

Synthesis of 1,4-dibromo-2,5-bis((2-ethylhexyl)oxy)-2,5-diethynylbenzene (1). A mixture of potassium carbonate (4.0 g, 28.97 mmol) and 2-ethylhexyl bromide (8.24 g, 40.55 mmol) was dissolved in 40 mL DMF under nitrogen. 2,5-Dibromohydroquinone (3.88 g, 14.48 mmol) was added slowly to this mixture, and the resulting reaction solution was stirred at 100 °C for 48 h. The mixture was then cooled to room temperature and quenched with water. The reaction mixture was extracted with dichloromethane, and the organic phase was washed with water, dried over Na_2SO_4, filtered, and evaporated to dryness to give the crude product. The crude was then purified by column chromatography on silica gel using hexane as the eluent to give compound **1** as a colorless oil (6.9 g, 97%). ^1H NMR (400 MHz, $CDCl_3$) δ 7.09 (s, 2H), 3.83 (d, 4H, J = 8.0 Hz), 1.76 (m, 2H, J = 12.0 Hz), 1.43–1.57 (m, 8H), 1.32–1.35 (m, 8H), 0.91–0.96 (m, 12H). ^{13}C NMR (100 MHz, $CDCl_3$): 150.1, 118.1, 111.0, 72.5, 39.4, 30.4, 29.0, 23.8, 23.0, 14.1, 11.1.

Synthesis of ((2,5-bis((2-ethylhexyl)oxy)-1,4-phenylene)bis(ethyne-2,1-diyl))bis(trimethylsilane) (2). A mixture of 1,4-dibromo-2,5-bis((2-ethylhexyl)oxy)-2,5-diethynylbenzene (**1**) (2.0 g, 4.06 mmol), $Pd(PPh_3)_2Cl_2$ (0.1.71 g, 0.243 mmol), and CuI (0.039 g, 0.203 mmol) in Et_3N (40 mL) was stirred for 5 minutes. Next, ethynyltrimethylsilane (1.0 g, 10.16 mmol) was added, and the reaction was heated at 90 °C under nitrogen for 48 h. Then, the reaction mixture was cooled down to room temperature and filtered; the filtrate was evaporated to dryness to yield a crude product. The crude product was then purified by column chromatography on silica gel using hexane : ethylacetate (30 : 1) as the eluent to give compound **2** as a yellow oil (1.69 g, 79%). ^{1}H NMR (400 MHz, $CDCl_3$) δ 6.89 (s, 2H), 3.81–3.86 (dd, 4H), 1.72–1.75 (m, 2H, J = 12.0 Hz), 1.44–1.58 (m, 8H), 1.32–1.34 (m, 8H), 0.91–0.96 (m, 12H), 0.26 (s, 18H).

Synthesis of 1,4-bis((2-ethylhexyl)oxy)-2,5-diethynylbenzene (3). The suspension of ((2,5-bis((2-ethylhexyl)oxy)-1,4-phenylene)bis-(ethyne-2,1-diyl))bis(trimethylsilane) (**2**) (0.29 g, 0.55 mmol) and KOH (0.93 g, 16.51 mmol) in THF : methanol (9 : 1) (30 mL) was stirred at room temperature for 1 h. Then, the reaction was quenched with water, and the resulting mixture was extracted with dichloromethane. The organic phase was washed with water, dried over Na_2SO_4, filtered, and evaporated to dryness to give compound **3** as a yellow oil–solid (0.21 g, 100% yield). ^{1}H NMR (400 MHz, $CDCl_3$): δ 6.96 (s, 2H), 3.85–3.86 (d, 4H, J = 4.0 Hz), 3.33 (s, 2H), 1.75–1.78 (m, 2H), 1.46–1.57 (m, 8H), 1.27–1.34 (m, 8H), 0.91–0.96 (m, 12H).

Synthesis of 8-(2-bromothien-5-yl)-3,5-dimethyl-4,4-difluoro-4-bora-3*a*,4*a*-diaza-*s*-indacene (BDY-Th-Br). Trifluoroacetic acid (TFA) (4 drops) was added to a solution of 5-bromo-2-thiophenecarbaldehyde (0.90 g, 4.70 mmol) and 2-methylpyrrole (0.86 g, 10.64 mmol) in degassed CH_2Cl_2 (300 mL), and the resulting mixture was stirred at room temperature overnight. Next, 2,3-dichloro-5,6-dicyano-1,4-benzoquinone (DDQ) (1.06 g, 4.70 mmol) was added, and the reaction mixture was stirred for an additional 2.5 h. Finally, *N*,*N*-diisopropylethylamine (i-Pr)$_2$EtN (1.33 g, 10.31 mmol) and boron trifluoride diethyl etherate ($BF_3{\cdot}Et_2O$) (2.33 g, 16.44 mmol) were added, and the reaction mixture was stirred for an additional 2 h. The reaction mixture was poured into water and extracted with CH_2Cl_2. The organic phase was dried over Na_2SO_4, filtered, and evaporated to dryness to give a crude product, which was further purified by column chromatography on silica gel using CH_2Cl_2 : hexanes (2 : 1) as the eluent. The pure product was obtained as a crystalline red solid (0.78 g, 44% yield). M.p. 132–133 °C. ^{1}H NMR (400 MHz, $CDCl_3$): δ 7.18 (m, 2H), 7.05 (d, 2H, J = 4.0 Hz), 6.31 (d, 2H, J = 4.0 Hz), 2.66 (s, 6H). ^{13}C NMR (100 MHz, $CDCl_3$): 15.0, 116.9, 119.7, 130.1, 130.6, 131.7, 133.2, 133.9, 136.1, 158.2.

Synthesis of 10-(5-((4-((5-(5,5-difluoro-3,7-dimethyl-5*H*-4l4,5l4-dipyrrolo[1,2-*c*:2′,1′-*f*][1,3,2]diazaborinin-10-yl)thiophen-2-yl)ethynyl)-2,5-bis((2-ethylhexyl)oxy)phenyl)ethynyl)thiophen-2-yl)-5,5-difluoro-3,7-dimethyl-5*H*-4l4,5l4-dipyrrolo[1,2-*c*:2′,1′-*f*][1,3,2]diazaborinine (BDY-PhAc-BDY). The reagents 8-(2-bromothien-5-yl)-3,5-dimethyl-4,4-difluoro-4-bora-3*a*,4*a*-diaza-*s*-indacene (**BDY-Th-Br**) (0.675 g, 1.77 mmol), CuI (0.0076 g, 0.040 mmol) and $Pd(PPh_3)_2Cl_2$ (0.056 g 0.08 mmol) in Et_3N : THF (2 : 1) (21 mL) were stirred for 5 minutes. Then, 1,4-bis((2-ethylhexyl)oxy)-2,5-diethynylbenzene (**3**) (0.308 g, 0.8 mmol) in 5 mL of THF was added, and the resulting mixture was heated at 80 °C under nitrogen for 24 h. Then, the reaction mixture was cooled to room temperature and evaporated to dryness. The crude was then purified by column chromatography on silica gel using dichloromethane as the eluent to give the pure product as a dark red solid (0.228 g, 29%). ^{1}H NMR (400 MHz, $CDCl_3$): δ 7.34 (m, 4H), 7.09 (d, 4H, J = 4.0 Hz), 7.02 (s, 2H), 6.33 (d, 4H, J = 4.0 Hz), 3.94 (m, 4H), 2.67 (s, 12.0 H), 1.80 (m, 2H), 1.52–1.58 (m, 8H), 1.27–1.36 (m, 8H), 0.98 (t, 6H), 0.90 (t, 6H). ^{13}C NMR (100 MHz, $CDCl_3$): δ 158.0, 153.9, 136.0, 134.0, 133.6, 132.0, 131.6, 130.2, 127.9, 119.6, 116.0, 113.7, 93.1, 87.5, 72.0, 39.6, 30.7, 29.1, 24.1, 23.1, 15.0, 14.1, 11.4. M.p. = 196–197 °C. MS(MALDI-TOF) m/z (M^+): calcd for $C_{56}H_{60}B_2F_4N_4O_2S_2$: 982.43, found: 983.302 $[M + H]^+$, 963.534 $[M - F]^+$, 870.685 $[M - 1 \times (2\text{-EH})]^+$, 758.961 $[M - 2 \times (2\text{-EH})]^+$. Anal. calcd for $C_{56}H_{60}B_2F_4N_4O_2S_2$: C, 68.43; H, 6.15; N, 5.70, found: C, 68.78; H, 6.25; N, 5.74.

Device fabrication and characterization

The OTFTs were fabricated by the bottom-gate/top-contact (BG/TC) structure. Highly n-doped silicon wafers (capacitance per unit area C_i = 11.4 nF cm^{-2}) with a thermally oxidized 300 nm SiO_2 layer were cleaned *via* acetone sonication for 10 min and oxygen plasma cleaning for 5 min (Harrick plasma, PDC-32G, 18 W). The organic layers of **BDY-PhAc-BDY** were deposited *via* solution-shearing on PS-brush-treated substrates. The PS-brush (M_w = 10 kg mol^{-1}) treatments were implemented by the general recipe[24] and the solution-shearing process was accomplished as the reported procedure.[25] The solution-sheared substrates were annealed in a vacuum oven at 100 °C for 24 h to remove the residual solvent. The concentration of the **BDY-PhAc-BDY** solution (1–2 mg mL^{-1}), solvent type, substrate temperature (50–80% of the solvent boiling point), and shearing speed (0.5–8 mm min^{-1}) were optimized. The thickness of organic films (40–62 nm) was measured by a profilometer (DEKTAK-XT, Brucker). The Au layers (40 nm) with various channel widths (W; 1000 and 500 μm) and lengths (L; 100 and 50 μm) were thermally evaporated to define the source and drain electrodes. The electronic performances of the OTFTs were characterized under vacuum conditions ($<10^{-2}$ Torr) at room temperature with a probe station (Keithely 4200-SCS). The microstructure and surface morphology of thin-films were measured by an atomic force microscope (AFM, NX10, Park systems), a scanning electron microscope (SEM, JSM-6010LA, JEOL), and X-ray diffraction (XRD, Smartlab, Rigaku).

Results and discussion

Synthesis, single-crystal structure and thermal characterizations

The synthesis of **BDY-PhAc-BDY** is shown in Scheme 1. 2,5-Dibromohydroquinone was first reacted with 2-ethylhexyl-bromide (2EH-Br) in the presence of K_2CO_3 base in DMF to yield the double alkylated product **1** in 97% yield. Double alkynylation reaction of **1** was performed *via* a Sonogashira

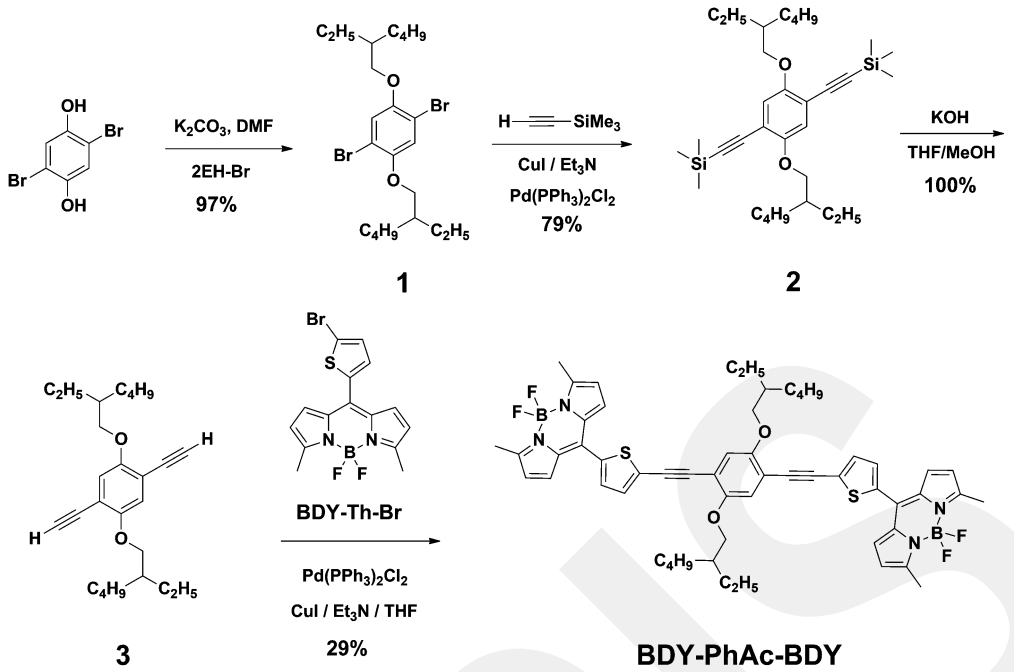

Scheme 1 Synthetic route to **BDY-PhAc-BDY**.

cross-coupling reaction with ethynyltrimethylsilane (HC≡C–$SiMe_3$) using the $Pd(PPh_3)_2Cl_2$ catalyst in the presence of CuI/Et_3N. This reaction yielded **2** in 79% yield, which then underwent quantitative (100% yield) desilylation with KOH to form hydrogen-ended ethynyl groups in compound **3**. In the final Sonogashira cross-coupling reaction, **3** was reacted with **BDY-Th-Br** in the presence of $Pd(PPh_3)_2Cl_2$ catalyst and CuI/Et_3N cocatalyst/base mixture. Note that **BDY-Th-Br** was prepared in accordance with our reported procedure.[20] Owing to the good solubility of the target small molecule in common organic solvents, the purification was carried out *via* column chromatography using $CHCl_3$ as eluent (29% yield). The chemical structure and purity of the intermediate compounds and the resulting small molecule, **BDY-PhAc-BDY**, were characterized by $^1H/^{13}C$ NMR (Fig. S1–S6, ESI†), MALDI-TOF (Fig. S7, ESI†), and Elemental analysis. Diffraction-quality single-crystals of **BDY-PhAc-BDY** were obtained by the diffusion of methanol into a chloroform solution at room temperature, and the corresponding solid-state structure was confirmed by single-crystal X-ray analysis (Fig. 2). **BDY-PhAc-BDY** is crystallized in the triclinic space group $P\bar{1}$ and it is located on a crystallographic inversion center. The BODIPY frame (C_9BN_2) adopts a nearly coplanar π-structure with the boron atom locating slightly out of this plane by 0.159(10) Å. As shown in Fig. 2B, the BODIPY π-core shows a dihedral angle ($\theta_{dihedral}$) of 44.94° with the *meso*-thiophene ring, which is slightly smaller than our previously reported "BODIPY-thiophene" dihedral angle (48.80°).[20] Moreover, this is much smaller than those measured between the dipyrrin framework and the *meso*-phenyl and thienyl units in previously reported BODIPY small molecules ($\theta_{dihedral}$ > 54–90°).[19,26–28] This co-planarization reflects the structural advantages of the current π-system, including the absence of β-pyrrole substitutions and the sterically confined nature of the five-membered thiophene ring.[29] The B1–F1 (1.385(11) Å) and B1–F2 (1.378(10) Å) bond distances and F1–B1–F2 (110.1(7)°), N1–B1–N2 (106.8(7)°), and N–B–F (av. 109.975°) bond angles are similar to those found in the literature.[30] As shown in Fig. 2C, the detailed crystal packing analysis of **BDY-PhAc-BDY** indicates that the presence of 2-ethylhexyloxy moieties on the central benzene ring prevents the π–π stacking interactions from occurring between the complete molecular π-backbones. However, BODIPY π-cores are still found to employ antiparallel arranged, π-stacked dimers with an interplanar distance of 3.93 Å in the unit cell (Fig. 2D). This arrangement is most likely a result of the energetically favorable antiparallel dipole–dipole interactions between the BODIPY cores' strong molecular dipole moments (μ = 3.38 Debye)[17] oriented toward the 4,4-fluorine substituents. In addition, relatively weaker "π···π" (~4.51 Å) interactions were observed between ethynyl (–C≡C–) groups, which, in combination with the strong edge-to-face "C–H···π (dialkoxyphenylic) (~2.85 Å)" interactions between π-electron-deficient BODIPY-pyrrole hydrogens and the central π-electron-rich dialkoxybenzene ring or ethynyl (–C≡C–) group, are found to play a critical role not only in solid-state formation, but also in thin-film crystallization to form highly crystalline microribbons (Fig. 5C, *vide infra*).

As shown in Fig. 3, **BDY-PhAc-BDY** was found to be highly thermally stable with the thermolysis onset temperature (5% mass loss) located at 300 °C. A two-step decomposition behavior was observed with a small step at ~87% of the original weight, corresponding to the mass loss of one of the alkyl substituents (–$CH_2CH(C_2H_5)(C_4H_9)$). Differential scanning calorimetry (DSC) measurements show a sharp endothermic peak at 198 °C with an enthalpy of 62.65 J g^{-1}. This peak indicates the thermal transition of the crystalline **BDY-PhAc-BDY** solid into

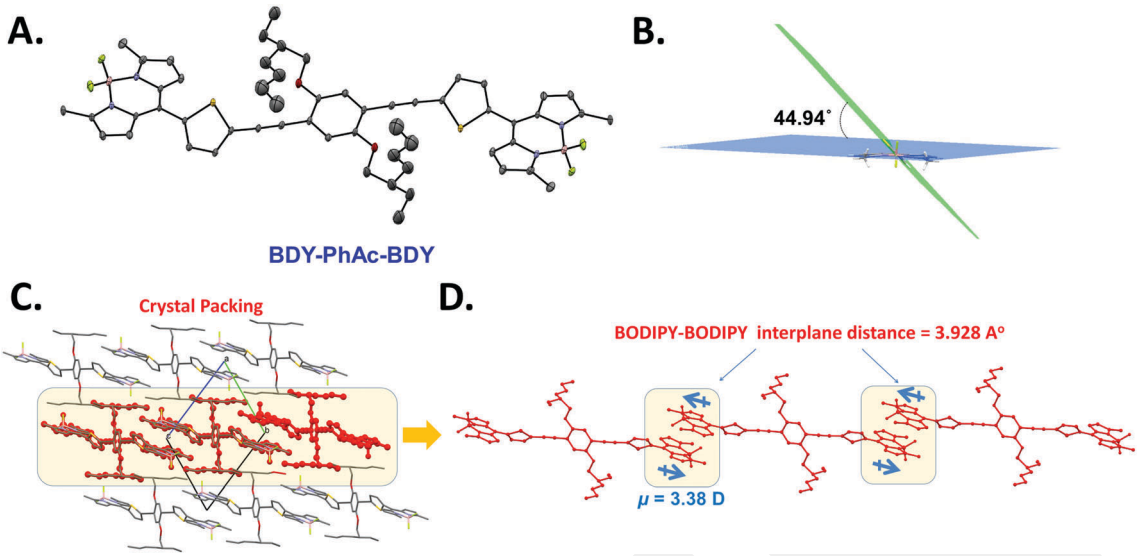

Fig. 2 (A) X-ray crystal structure of **BDY-PhAc-BDY** with 20% ellipsoids. The grey, blue, red, pink, yellow, and white coloured atoms represent C, N, O, B, F, and H, respectively, (B) perspective view of the inter-ring dihedral angle between boron-dipyrromethene and the *meso*-aromatic unit planes, (C) crystal packing of **BDY-PhAc-BDY**, and (D) perspective view of antiparallel arranged, π-stacked dimers (3.928 Å), which occurred between two BODIPY units. The local dipole moments (μ = 3.38 Debye) of the BODIPY cores are shown in blue.

an isotropic liquid, which was further confirmed by a conventional melting-temperature measurement ($T_{m.p.}$ = 196–197 °C). This is very different from our previously reported non-substituted BODIPY-small molecules, **BDY-3T-BDY**/**BDY-4T-BDY**, which showed thermal decompositions with no observable melting points.[20] This reflects the critical role of flexible swallow-tailed 2-ethylhexyloxy substituents in tuning intermolecular interactions, which eventually induces the melting process. Note that once the crystalline solid obtained from chromatographic purification melts to an isotropic liquid, no corresponding crystallization peak is observed in the cooling cycle. This indicates that **BDY-PhAc-BDY** adopts an amorphous solid-state upon cooling and it does not exhibit a further melting peak in the second-heating cycle (Fig. 3B).

Optical and electrochemical properties

The electrochemical and optical properties of **BDY-PhAc-BDY** were evaluated by UV-vis absorption and photoluminescence spectroscopies, and cyclic voltammetry. **BDY-PhAc-BDY** exhibits two absorption peaks in dichloromethane solution with λ_{max} located at 355 nm and 527 nm. The large molar extinction coefficient ($\varepsilon = 1 \times 10^5$ M^{-1} cm^{-1}) for the absorption peak at 527 nm and the out-of-plane vibronic feature at 495 nm ($\approx$1200 cm^{-1} shift from λ_{max}) are unique features of the BODIPY-based π–π* ($S_0 \rightarrow S_1$) transition.[15] The broad peak with a lower intensity at 355 nm is ascribed to a combination of BODIPY-based $S_0 \rightarrow S_2$ and 1,4-bis-(thienylethynyl)2,5-dialkoxybenzene-based π–π* transitions. The optical band gap is

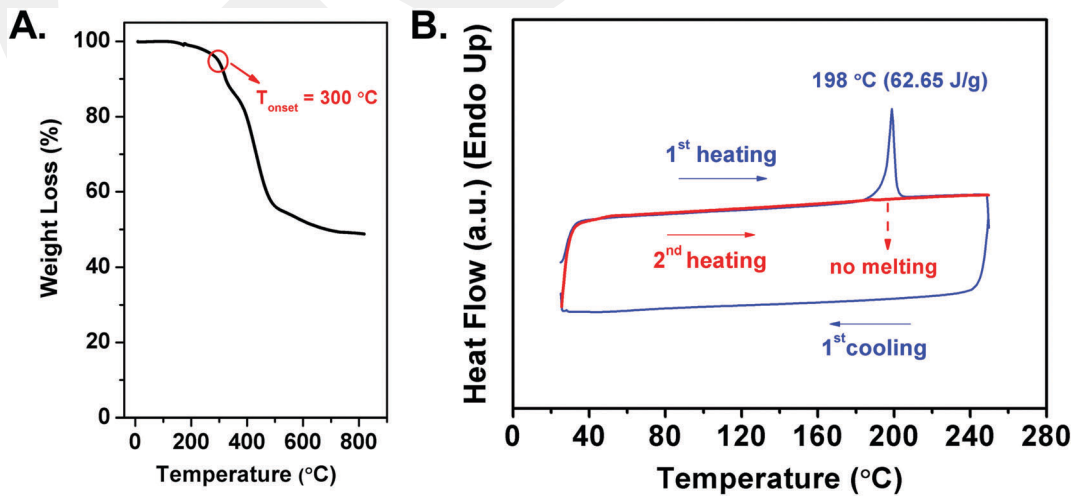

Fig. 3 (A) Thermogravimetric analysis (TGA), and (B) differential scanning calorimetry (DSC) measurement curves of **BDY-PhAc-BDY** at a temperature ramp of 10 °C min^{-1} under N_2.

estimated as 2.22 eV from the low-energy absorption edge. In the thin-film state (spin-coated on a glass substrate), the absorption maxima show bathochromic shifts (λ_{max} = 365/543 nm) and the optical band gap is lowered to 2.06 eV (solid-state) with respect to those in the solution. This is indicative of molecular π-backbone planarization and solid-state ordering as compared to the solution phase. The fluorescence spectrum of **BDY-PhAc-BDY** in dichloromethane solution (Fig. S8, ESI†) exhibits a broad emission peak with considerably shifted maximum at 646 nm (Stokes shift = 119 nm) and a very low quantum yield (Φ_F) of ~0.02%. This is very different from typical BODIPY emission features, such as high quantum yield and extremely low Stokes shifts, and it most likely reflects the presence of nonradiative pathways in the excited state *via* intra-/inter-molecular charge transfer processes.[31] When the solvent dielectric constant was lowered (THF (ε = 8.9) → toluene (ε = 2.3)), a highly blue-shifted PL spectrum was measured in toluene (Fig. S8, ESI,† λ_{em} = 578 nm), indicating positive solvachromatism. This further confirms that the final relaxed excited state employs a large dipole moment as a result of charge transfer (CT) between the subchromophoric units. Based on the DFT calculations (B3LYP/6-31G** level of theory), the lowest unoccupied molecular orbital (LUMO) of **BDY-PhAc-BDY** is found to be symmetrically localized on the outer BODIPY π-acceptor units, while the highest occupied molecular orbital (HOMO) is delocalized only on the central π-donor part, with noticeable contributions from the oxygens on the alkoxy groups (Fig. 4, inset). This further supports the emission characteristics of **BDY-PhAc-BDY**—that the photo-excitation is probably accompanied by an intramolecular charge-transfer (CT) in the excited state from the donor to the acceptor unit (HOMO → LUMO). Cyclic voltammetry measurements reveal two reversible reductions and one quasi-reversible oxidation for **BDY-PhAc-BDY**, with the first half-wave reduction-potential ($E_{1/2}^{red\text{-}1}$) located at −0.84 V and the first onset oxidation-potential ($E_{onset}^{ox\text{-}1}$) located at 1.28 V. The electrochemical band gap (2.12 eV) shows excellent agreement with the optical band gap (2.22 eV) measured in solution. The HOMO and LUMO energy levels are estimated as −5.68 eV and −3.56 eV, respectively. Note that as a result of π-electron deficiency of the *meso*-substituted BODIPYs at the molecular termini, the LUMO energy level of the new molecule is sufficiently stabilized to be in the energetic range of previously reported n-channel semiconductors (−2.9 to −4.3 eV).[32] Furthermore, when compared with the observed p-doping characteristics, the highly reversible and favorable reductive properties of **BDY-PhAc-BDY** are indicative of its electron-transporting semiconductor potential.

Thin-film microstructure/morphology and field-effect transistor characterization

Semiconductor thin-films (40–62 nm) were fabricated by solution-shearing **BDY-PhAc-BDY** solution in 1,2,4-trichlorobenzene (1.0 mg mL^{-1}) on PS (polystyrene)-brush treated n^{++}-Si/SiO$_2$ substrates. Bottom-gate/top-contact (BG/TC) OFETs were completed by thermal evaporation of the source and drain Au electrodes (40 nm) *via* thermal evaporation (deposition rate = 0.2 Å s^{-1}) to yield various channel lengths (L: 100 and 50 μm) and widths (W: 1000 and 500 μm). The microstructure of the solution-sheared **BDY-PhAc-BDY** thin-film was investigated by out-of-plane X-ray diffraction measurement, which displays a major diffraction peak at 2θ = 8.94° (Fig. 5A). The second and third order diffractions of the same crystalline phase were also observed revealing a high degree of ordering across the thin-film thickness. The simulation of the powder pattern based on the single-crystal structure of **BDY-PhAc-BDY** (Fig. S9, ESI†) shows that all these peaks are well indexed along the (010) lattice plane, and second and third order diffractions

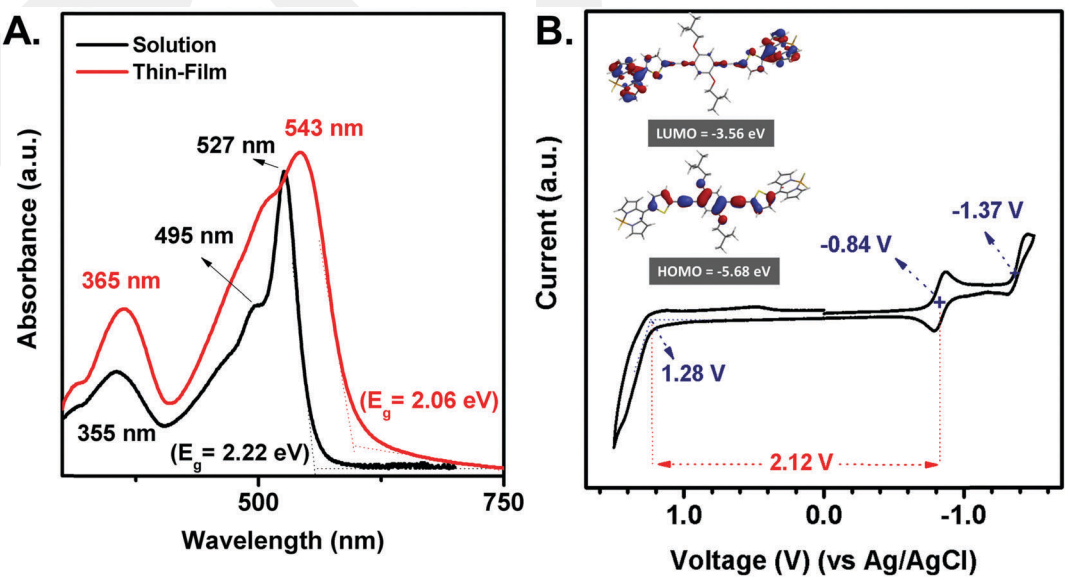

Fig. 4 (A) Optical absorption in dichloromethane solution (black line) and as a thin-film (red line) of **BDY-PhAc-BDY**, and (B) cyclic voltammogram of **BDY-PhAc-BDY** in dichloromethane (0.1 M $Bu_4N^+PF_6^-$, scan rate = 50 mV s^{-1}). Inset: The calculated (DFT, B3LYP/6-31G**) topographical orbital representations and experimentally estimated HOMO and LUMO energy levels.

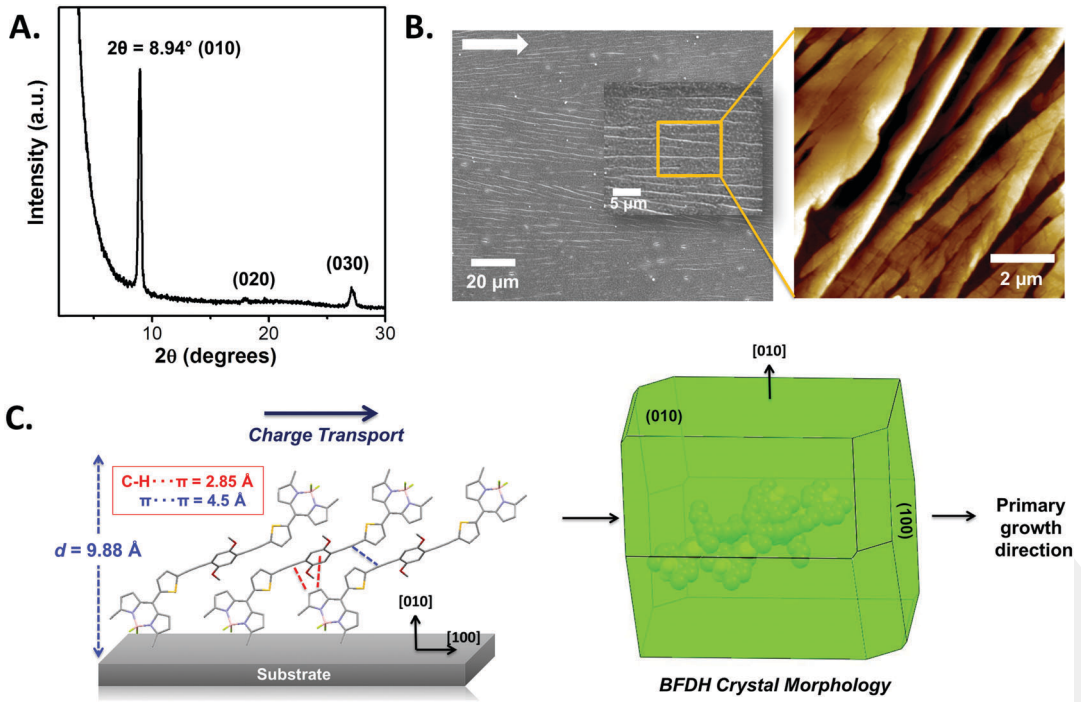

Fig. 5 θ–2θ X-ray diffraction (XRD) scans (A) and SEM/AFM-topographic images (B) of the solution-sheared **BDY-PhAc-BDY** thin-film. (C) The molecular arrangement in the out-of-plane [010] direction and the BFDH (Bravais, Friedel, Donnay and Harker) theoretical crystal morphology showing the primary crystal growth direction ([100]). The arrow shows the shearing direction. "–CH···π" contacts (~2.85 Å) and "π···π" (~4.5 Å) interactions are shown between two representative molecules.

correspond to (020) and (030), respectively. The periodicity (*d*-spacing) of the (010) plane in the thin-film phase is measured as 9.88 Å, which corresponds to "*b*-axis (10.928 Å) × sin α(66.26°)" and suggests that the molecules adopt a highly tilted molecular orientation on the substrate (Fig. 5C). Atomic force microscopy (AFM) and scanning electron microscopy (SEM) characterizations show that the morphology of the solution-sheared thin-film of **BDY-PhAc-BDY** consisted of one-dimensional (1-D) highly crystalline micron-sized ribbons, which were perfectly aligned along the shearing direction (Fig. 5B). The lengths of the microribbons reached ~0.1 mm and their widths were ~0.5–2.0 μm. Detailed analysis of the AFM image also shows the formation of well-connected smaller grains with ~200–500 nm lengths along the ribbon long-axis. In order to elucidate the structural packing in these micro-ribbons, the BFDH (Bravais, Friedel, Donnay, and Harker) theoretical crystal morphology was used, which predicts a high aspect ratio crystal growth perpendicular to the [010] out-of-plane direction. Since the self-assembly process during thin-film crystallization may be similar to single-crystal formation, the thermodynamically/kinetically more favored primary crystal growth along the [100] crystallographic direction most likely reflects the anisotropic ribbon growth due to similar directional intermolecular forces.[33–35] This shows that the major intermolecular interactions governing thin-film crystallization are: (i) strong "–CH···π" contacts (~2.85 Å) between π-deficient BODIPY-pyrrole hydrogens and the central π-electron rich dialkoxybenzene ring/ethynyl (–C≡C–) groups, (ii) "π···π" (~4.5 Å) interactions between the ethynyl (–C≡C–) groups, and (iii) "π···π" (~3.9 Å) and dipole–dipole interactions between antiparallel arranged BODIPY frameworks (*vide infra*). It appears to us that the directional solution-shearing process used for the current thin-film fabrications might also play a key role in facilitating **BDY-PhAc-BDY**'s molecular self-assembly into anisotropic ribbons along the shearing direction.[25] The formation of a ribbon-like morphology with the solution-shearing method is consistent with our previous rod-like BODIPY small molecules (**BDY-3T**/**4T-BDY**), which also yielded high-aspect ratio microfibers in thin-film.

OFET device characteristics were measured with a Keithley 4200-SCS semiconductor characterization system at room temperature. The transistor characteristics in the saturation regime, such as charge carrier mobilities (μ) and threshold voltages (V_T), were extracted from the equation:

$$\mu_{sat} = (2I_{DS}L)/[WC_i(V_G - V_T)^2]$$

where I_{DS} is the drain current, L and W are the channel length and width, respectively, C_i is the areal capacitance of the gate dielectric, V_G is the gate voltage, and V_T is the threshold voltage. Typical transfer and output curves are shown in Fig. 6 and S10 (ESI†). Consistent with the theoretical and experimental optoelectronic characterizations on the small molecule (*vide supra*), these devices exhibited n-channel behavior with μ_e = 0.004 cm^2 V^{-1} s^{-1} and I_{on}/I_{off} = 10^5–10^6. This clearly shows that BODIPY is an effective π-acceptor unit to afford substantial lowering of the LUMO level and to induce n-channel semiconductivity in π-conjugated small molecules for use in optoelectronic devices. Although the current electron mobility for the **BDY-PhAc-BDY** thin-film is

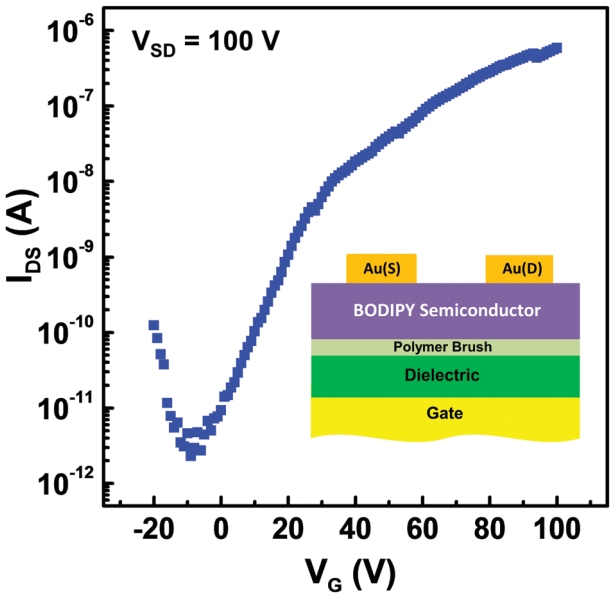

Fig. 6 Representative transfer plot in the n-channel region for bottom-gate/top-contact (BG/TC) OFET devices fabricated with solution-sheared **BDY-PhAc-BDY** thin-film.

much lower than the state-of-the-art performances achieved previously with other molecular π-systems, it is still remarkable from a molecular design perspective since it is the highest reported to date for a BODIPY-based small molecular semiconductor with alkyne linkages. Besides, the growth of well-oriented micro- and nano-sized organic semiconductor structures from the solution phase has always been challenging in the literature and it offers great advantages in the fabrication of transistor arrays for circuit design.[34,36] Although π–π stacking between whole molecular skeletons is not evident along the charge-transport (in-plane) direction, the localized π–π stackings between individual acceptor or donor units in the twisted arrangement of A–D–A π-architecture,[37] and strong "–CH···π" interactions in the face-to-edge herringbone packing, may still contribute to 3-D charge transport, which, along with the highly-crystalline microstructure, explains the observed mobility. Since the thin-film crystallinity and morphology of the current semiconductor remains similar to our previously reported non-substituted semiconductor, **BDY-4T-BDY**, the slightly reduced (2.5×) OFET performance is most likely related to the presence of σ-insulating alkyl substituents on the central benzene ring. Based on our findings, note that the BODIPY π-core offers a unique advantage by providing good solubility to the molecular π-system even in the absence of an alkyl substituent. Therefore, for the future development of solution-processable BODIPY-based semiconductors, we rationalize that non-substituted systems should be preferred to yield higher mobilities.

Conclusions

A new solution-processable BODIPY-acetylene small molecule, **BDY-PhAc-BDY**, based on A–D–A π-architecture was designed, synthesized and fully characterized. The new semiconductor exhibited a low solid-state optical band gap of 2.06 eV with stabilized HOMO and LUMO energy levels of −5.68 eV and −3.56 eV, respectively. Single-crystal X-ray diffraction (XRD) analysis revealed crucial structural features and intermolecular interactions, such as a relatively small "BODIPY-*meso*-thiophene" dihedral angle ($\theta_{dihedral}$ = 44.94°) and antiparallel π-stacked BODIPY dimers with an interplanar distance of 3.93 Å. Highly crystalline one-dimensional (1-D) microribbons of **BDY-PhAc-BDY** were grown from the chloroform solution on PS (polystyrene)-brush treated substrates *via* a solution-shearing method. Strong edge-to-face "C–H(pyrrolic)···π(dialkoxyphenylic) (∼2.85 Å)" and relatively weaker "π(ethynyl)···π(ethynyl)" (∼4.51 Å) directional interactions were found to be effective in the formation of current highly crystalline microribbons along the [100] direction. The bottom-gate/top-contact OFET devices based on these microribbons exhibited clear n-channel operation and afforded an electron mobility of 0.004 $cm^2 V^{-1} s^{-1}$ and an on/off current ratio of 10^5–10^6, which is the highest reported to date for BODIPY-based small molecular semiconductors with alkyne linkages. Our findings clearly demonstrate that BODIPY is an effective π-acceptor unit for the realization of solution-processable donor–acceptor type small molecules for electron-transport. Here, we also offer crucial guidance for the design of future BODIPY-based semiconductor molecules with further improved electrical performances, and easily fabricable 1-D semiconductor thin-film morphologies for fundamental/applied research in organic optoelectronics.

Acknowledgements

H. U. acknowledges support from TUBITAK 114M226 and the Turkish Academy of Sciences' Young Scientists Award Program (TUBA-GEBİP 2015). C. K. acknowledges support from the National Research Foundation of Korea (NRF) (2016K1A3A1A31905000).

References

1 H. Ebata, T. Izawa, E. Miyazaki, K. Takimiya, M. Ikeda, H. Kuwabara and T. Yui, *J. Am. Chem. Soc.*, 2007, **129**, 15732–15733.
2 R. Capelli, S. Toffanin, G. Generali, H. Usta, A. Facchetti and M. Muccini, *Nat. Mater.*, 2010, **9**, 496–503.
3 A. Facchetti, *Chem. Mater.*, 2011, **23**, 733–758.
4 J. Li, Y. Zhao, H. S. Tan, Y. Guo, C.-A. Di, G. Yu, Y. Liu, M. Lin, S. H. Lim, Y. Zhou, H. Su and B. S. Ong, *Sci. Rep.*, 2012, **2**, 754.
5 H. E. Katz, Z. Bao and S. L. Gilat, *Acc. Chem. Res.*, 2001, **34**, 359–369.
6 L. Chua, J. Zaumseil, J. Chang, E. C.-W. Ou, P. K.-H. Ho, H. Sirringhaus and R. H. Friend, *Nature*, 2005, **434**, 194–199.
7 M.-C. Chen, S. Vegiraju, C.-M. Huang, P.-Y. Huang, K. Prabakaran, S. L. Yau, W.-C. Chen, W.-T. Peng, I. Chao, C. Kim and Y.-T. Tao, *J. Mater. Chem. C*, 2014, **2**, 8892–8902.
8 S. Allard, M. Forster, B. Souharce, H. Thiem and U. Scherf, *Angew. Chem., Int. Ed.*, 2008, **47**, 4070–4098.

9 M. Sawamoto, M. J. Kang, E. Miyazaki, H. Sugino, I. Osaka and K. Takimiya, *ACS Appl. Mater. Interfaces*, 2016, **8**, 3810–3824.
10 R. Ponce Ortiz, H. Herrera, M. J. Mancheño, C. Seoane, J. L. Segura, P. Mayorga Burrezo, J. Casado, J. T. López Navarrete, A. Facchetti and T. J. Marks, *Chem. – Eur. J.*, 2013, **19**, 12458–12467.
11 L. Zhang, A. Fonari, Y. Liu, A.-L. M. Hoyt, H. Lee, D. Granger, S. Parkin, T. P. Russell, J. E. Anthony, J.-L. Brédas, V. Coropceanu and A. L. Briseno, *J. Am. Chem. Soc.*, 2014, **136**, 9248–9251.
12 M. Durso, C. Bettini, A. Zanelli, M. Gazzano, M. G. Lobello, F. De Angelis, V. Biondo, D. Gentili, R. Capelli, M. Cavallini, S. Toffanin, M. Muccini and M. Melucci, *Org. Electron.*, 2013, **14**, 3089–3097.
13 K.-H. Kim, H. Yu, H. Kang, D. J. Kang, C.-H. Cho, H.-H. Cho, J. H. Oh and B. J. Kim, *J. Mater. Chem. A*, 2013, **1**, 14538.
14 H. Yu, H.-H. Cho, C.-H. Cho, K.-H. Kim, D. Y. Kim, B. J. Kim and J. H. Oh, *ACS Appl. Mater. Interfaces*, 2013, **5**, 4865–4871.
15 A. C. Benniston, G. Copley, A. Harriman and R. Ryan, *J. Mater. Chem.*, 2011, **21**, 2601.
16 A. Bessette and G. S. Hanan, *Chem. Soc. Rev.*, 2014, **43**, 3342.
17 H. Usta, M. D. Yilmaz, A. J. Avestro, D. Boudinet, M. Denti, W. Zhao, J. F. Stoddart and A. Facchetti, *Adv. Mater.*, 2013, **25**, 4327–4334.
18 A. M. Poe, A. M. Della Pelle, A. V Subrahmanyam, W. White, G. Wantz and S. Thayumanavan, *Chem. Commun.*, 2014, **50**, 2913.
19 T. Bura, N. Leclerc, S. Fall, P. Lévêque, T. Heiser, P. Retailleau, S. Rihn, A. Mirloup and R. Ziessel, *J. Am. Chem. Soc.*, 2012, **134**, 17404–17407.
20 M. Ozdemir, D. Choi, G. Kwon, Y. Zorlu, B. Cosut, H. Kim, A. Facchetti, C. Kim and H. Usta, *ACS Appl. Mater. Interfaces*, 2016, **8**, 14077–14087.
21 F. Silvestri, A. Marrocchi, M. Seri, C. Kim, T. J. Marks, A. Facchetti and A. Taticchi, *J. Am. Chem. Soc.*, 2010, **132**, 6108–6123.
22 *Acetylene Chemistry: Chemistry, Biology and Materials Science*, ed. F. Diederich, P. J. Stang and R. R. Tykwinski, Wiley-VCH, Weinheim, 2005.
23 M. J. Frisch, G. W. Trucks, H. B. Schlegel, G. E. Scuseria, M. A. Robb, J. R. Cheeseman, G. Scalmani, V. Barone, B. Mennucci, G. A. Petersson, H. Nakatsuji, M. Caricato, X. Li, H. P. Hratchian, A. F. Izmaylov, J. Bloino, G. Zheng, J. L. Sonnenberg, M. Hada, M. Ehara, K. Toyota, R. Fukuda, J. Hasegawa, M. Ishida, T. Nakajima, Y. Honda, O. Kitao, H. Nakai, T. Vreven, J. A. Montgomery, Jr., J. E. Peralta, F. Ogliaro, M. Bearpark, J. J. Heyd, E. Brothers, K. N. Kudin, V. N. Staroverov, T. Keith, R. Kobayashi, J. Normand, K. Raghavachari, A. Rendell, J. C. Burant, S. S. Iyengar, J. Tomasi, M. Cossi, N. Rega, J. M. Millam, M. Klene, J. E. Knox, J. B. Cross, V. Bakken, C. Adamo, J. Jaramillo, R. Gomperts, R. E. Stratmann, O. Yazyev, A. J. Austin, R. Cammi, C. Pomelli, J. W. Ochterski, R. L. Martin, K. Morokuma, V. G. Zakrzewski, G. A. Voth, P. Salvador, J. J. Dannenberg, S. Dapprich, A. D. Daniels, O. Farkas, J. B. Foresman, J. V. Ortiz, J. Cioslowski and D. J. Fox, *Gaussian 09, Revision C.01*, Gaussian, Inc., Wallingford CT, 2010.
24 S. H. Park, H. S. Lee, J.-D. Kim, D. W. Breiby, E. Kim, Y. D. Park, D. Y. Ryu, D. R. Lee and J. H. Cho, *J. Mater. Chem.*, 2011, **21**, 15580.
25 G. Giri, E. Verploegen, S. C. Mannsfeld, S. Atahan-Evrenk, H. Kim do, S. Y. Lee, H. A. Becerril, A. Aspuru-Guzik, M. F. Toney and Z. Bao, *Nature*, 2011, **480**, 504.
26 P. E. Kesavan, S. Das, M. Y. Lone, P. C. Jha, S. Mori and I. Gupta, *Dalton Trans.*, 2015, **44**, 17209–17221.
27 H. L. Kee, C. Kirmaier, L. Yu, P. Thamyongkit, W. J. Youngblood, M. E. Calder, L. Ramos, B. C. Noll, D. F. Bocian, W. R. Scheidt, R. R. Birge, J. S. Lindsey and D. Holten, *J. Phys. Chem. B*, 2005, **109**, 20433–20443.
28 A. C. Benniston, G. Copley, A. Harriman, D. B. Rewinska, R. W. Harrington and W. Clegg, *J. Am. Chem. Soc.*, 2008, **130**, 7174–7175.
29 Y. Yang, Q. Guo, H. Chen, Z. Zhou, Z. Guo and Z. Shen, *Chem. Commun.*, 2013, **49**, 3940.
30 D. Aydın Tekdaş, G. Viswanathan, S. Zehra Topal, C. Y. Looi, W. F. Wong, G. Min Yi Tan, Y. Zorlu, A. G. Gürek, H. B. Lee and F. Dumoulin, *Org. Biomol. Chem.*, 2016, **14**, 2665–2670.
31 M. T. Whited, N. M. Patel, S. T. Roberts, K. Allen, P. I. Djurovich, S. E. Bradforth and M. E. Thompson, *Chem. Commun.*, 2012, **48**, 284–286.
32 H. Usta, A. Facchetti and T. J. Marks, *Acc. Chem. Res.*, 2011, **44**, 501–510.
33 G. K. Veits, K. K. Carter, S. J. Cox and A. J. McNeil, *J. Am. Chem. Soc.*, 2016, **138**, 12228–12233.
34 M. Wang, J. Li, G. Zhao, Q. Wu, Y. Huang, W. Hu, X. Gao, H. Li and D. Zhu, *Adv. Mater.*, 2013, **25**, 2229–2233.
35 T. He, M. Stolte and F. Würthner, *Adv. Mater.*, 2013, **25**, 6951–6955.
36 H. Li, B. C.-K. Tee, J. J. Cha, Y. Cui, J. W. Chung, S. Y. Lee and Z. Bao, *J. Am. Chem. Soc.*, 2012, **134**, 2760–2765.
37 M. Gsänger, J. H. Oh, M. Könemann, H. W. Höffken, A.-M. Krause, Z. Bao and F. Würthner, *Angew. Chem., Int. Ed.*, 2010, **49**, 740–743.

